# Comparison of MIL-101(Cr) metal-organic framework and 13X zeolite monoliths for $CO_2$ capture

**Wan Yun Hong[a,1], Semali P. Perera[a], Andrew D. Burrows[b]**

[a] *Department of Chemical Engineering, University of Bath, Bath BA2 7AY, United Kingdom*

[b] *Department of Chemistry, University of Bath, Bath BA2 7AY, United Kingdom*

## ABSTRACT

A comparative study was conducted to determine the pore properties and adsorptive performance of monoliths containing either the MIL-101(Cr) metal-organic framework or 13X zeolite for carbon dioxide ($CO_2$) capture. Although there has been a great deal of previous work on $CO_2$ adsorption onto zeolites and MOFs, there has been far fewer studies on structured adsorbents such as monoliths. The results indicate that MIL-101(Cr) monoliths have 1.3 times higher porosity than 13X zeolite monoliths. Increasing $CO_2$ partial pressure in the gas mixture shortens breakthrough and equilibrium times and increases their breakthrough and equilibrium adsorption capacities of $CO_2$. MIL-101(Cr) monoliths show better mass transfer of $CO_2$ in the adsorbent bed with shorter breakthrough and equilibrium times of about 20% and 35%, respectively, than 13X zeolite monoliths. The adsorption capacity of $CO_2$ on MIL-101(Cr) monoliths is higher by about 37% (based on weight in mmol/g) at breakthrough and slightly lower by about 7% at equilibrium when compared to 13X zeolite monoliths. MIL-101(Cr) monoliths were found to be 1.5 times more efficient for $CO_2$ adsorption than 13X zeolite monoliths. The effects of regeneration temperature after $CO_2$ adsorption on MIL-101(Cr) and 13X zeolite monoliths were studied and results showed an increase in $CO_2$ adsorption capacity

[1] Corresponding author. Present address: Faculty of Integrated Technologies, Universiti Brunei Darussalam, Jalan Tungku Link, Gadong BE1410, Brunei Darussalam.

*E-mail address:* w.y.hong58@gmail.com (W.Y. Hong).

as the regeneration temperature was increased. In summary, the study showed MIL-101(Cr) monoliths have better $CO_2$ adsorption properties than 13X zeolite monoliths.

**Keywords:**

MIL-101(Cr) metal-organic framework, 13X zeolite, Monoliths, $CO_2$ capture, Adsorption

## 1. Introduction

Metal-organic frameworks (MOFs) are an emerging new class of porous materials that are being developed as alternative adsorbents for capturing carbon dioxide ($CO_2$) due to their high porosity, large pore size and surface area, good thermal and chemical stabilities, low framework density and high adsorption capacity for $CO_2$ [1,2,3]. One of the most promising MOFs is MIL-101(Cr), which is a porous crystalline material that is known for its capability for capturing $CO_2$ [4] and exhibits excellent hydrothermal stability [1,5] compared to many other MOFs [6,7]. It has a three-dimensional framework structure made up of trimeric chromium(III) ($Cr_3O$) aggregates joined to 1,4-benzenedicarboxylate (bdc) ligands with an internal cavity diameter up to 3.4 nm and a large Langmuir surface area of 5900 ± 300 $m^2/g$ [1]. Small-sized gas molecules such as $CO_2$ (average diameter of 0.36 nm) can be absorbed into the large cavities of MIL-101(Cr). Due to the strong adsorptive forces between the polar $CO_2$ gas molecules and the chromium aggregates on the surface of MIL-101(Cr), MIL-101(Cr) has showed high $CO_2$ adsorption capacities up to 8.00 mmol/g at 5.3 bar and 10 °C according to the pure $CO_2$ adsorption isotherm presented by Chowdhury et al. (2009) [4]. The structure of MIL-101(Cr) is stable up to 275 °C [1].

Many $CO_2$ gas adsorption studies on MIL-101(Cr) had been carried out in the forms of powder [8,9] or granules [10]. However, the powder form of an adsorbent is not practical for use in industry and the granular form of an adsorbent often creates high pressure drops in packed bed systems, which leads to high energy requirements [11] and inefficient adsorption

performance [12]. There are very few studies describing the use of MIL-101(Cr) monoliths for $CO_2$ gas adsorption and the first one was reported by Hong et al. in 2015 [13]. Many studies have used $CO_2$ capture adsorbents in powder form but the comparative adsorption study on MIL-101(Cr) and industry standard 13X zeolite in monolithic structures for $CO_2$ capture application has not been reported. These MIL-101(Cr) and 13X zeolite monoliths could have potential for use in industrial $CO_2$ capture applications.

The three-dimensional framework structure of 13X zeolite consists of a group of silicon and aluminium tetrahedra ($SiO_4$ and $AlO_4$) connected to twelve-membered oxygen rings and charged balanced by sodium cations ($Na^+$) to form an open crystal lattice [14]. The crystal lattice of 13X zeolite has hydrated cavities joined through pores of diameter 0.75 nm [15] that allow small gas molecules such as $CO_2$ to penetrate and adsorb in the cavities [16]. Additionally, 13X zeolite has strong adsorptive forces to attract polar molecules such as $CO_2$. A study by Cavenati et al. (2004) has demonstrated that 13X zeolite extrudates have a high $CO_2$ adsorption capacity of 6.50 mmol/g at 10 bar and 25 °C with a feed $CO_2$ concentration > 99.998% vol. [17]. 13X zeolite has high thermal stability and is stable to over 800 °C [18].

In this paper, MIL-101(Cr) and 13X zeolite monoliths are characterised by simultaneous thermogravimetric and differential scanning calorimetry, mercury intrusion porosimetry (MIP) and dynamic $CO_2$ adsorption breakthrough experiments. Adsorption properties such as breakthrough and equilibrium times, breakthrough and equilibrium adsorption capacities of $CO_2$ and effectiveness of the adsorbent bed utilised for $CO_2$ adsorption are determined by analysing their $CO_2$ adsorption breakthrough curves. Both MIL-101(Cr) and 13X zeolite monoliths are tested with a range of feed $CO_2$ gas concentrations (0.4% vol., 4% vol. and 40% vol.) at a constant pressure of 2 bar and feed gas flow rate of 500 mL/min. The adsorption performance of MIL-101(Cr) monoliths for $CO_2$ capture is compared with that of 13X zeolite monoliths. The effect of regeneration temperatures on $CO_2$ adsorption performance of MIL-101(Cr) and 13X zeolite monoliths is also investigated. The aim of the study is to assess the

adsorptive performance of MIL-101(Cr) monoliths in comparison with that of 13X zeolite monoliths for $CO_2$ capture application.

## 2. Experimental

### *2.1. Reagents and materials*

Chemicals for the synthesis of MIL-101(Cr) were chromium(III) nitrate nonahydrate (99%) and 1,4-benzenedicarboxylic acid (also known as terephthalic acid) (≥ 99%) that were purchased from Acros Organics (United Kingdom, UK). Ethanol (≥ 99.8%) was purchased from Sigma-Aldrich Co. (USA). Raw materials for the preparation of adsorbent monoliths include 13X zeolite powder (particle diameter between 3 μm and 5 μm) purchased from Zeochem AG (Switzerland), calcium bentonite powder (particle diameter < 0.5 μm) purchased from Bath Potters' Supplies Ltd. (UK) and licowax C micropowder PM (particle diameter of 15.1 μm) purchased from Clariant (UK). The non-wetting liquid for pore characterisation was mercury and it was purchased from Sigma-Aldrich Co. (USA). The model $CO_2$ gas concentrations for the dynamic adsorption experiments were 0.4% vol., 4% vol. and 40% vol. $CO_2$ in air and they were purchased from BOC Ltd. (UK). All substances were used as obtained from commercial sources.

### *2.2. Synthesis of MIL-101(Cr)*

MIL-101(Cr) was synthesised by hydrothermal reaction of chromium(III) nitrate nonahydrate (4.2 g), 1,4-benzendicarboxylic acid (1.6 g) and distilled water (49 mL) at 220 °C for 8 hours. Then, the mixture was cooled to room temperature. The resulting green precipitate was separated by centrifugation, washed with distilled water and dried at room temperature. To remove unreacted 1,4-benzenedicarboxylic acid from the pores of MIL-101(Cr), the crude product was treated with ethanol at 80 °C for 4 hours. The mixture was cooled to room

temperature and then the product was separated by centrifugation, washed with ethanol and dried at room temperature.

### *2.3. Preparation of MIL-101(Cr) and 13X zeolite monoliths*

Both MIL-101(Cr) and 13X zeolite monoliths were prepared by a paste extrusion technique that comprises five processing steps, which are: (1) adsorbent paste preparation, (2) pre-drying, (3) extrusion, (4) drying and (5) firing (Fig. 1). In the first processing step, MIL-101(Cr) and 13X zeolite pastes were prepared individually by mixing MIL-101(Cr) powder or 13X zeolite powder and calcium bentonite powder with an adsorbent to clay ratio of 75:25 (in dry weight). To enhance the structural porosity of MIL-101(Cr) and 13X zeolite monoliths, licowax C micropowder PM (4% of total dry weight) was added to MIL-101(Cr) and 13X zeolite paste mixtures. Water was used for mixing the paste (150% of total dry weight for MIL-101(Cr) paste and 116% of total dry weight for 13X zeolite paste). After the MIL-101(Cr) and 13X zeolite pastes were prepared, they were allowed to mature at room temperature. In this pre-drying step, excess water in the adsorbent pastes slowly evaporates.

Once MIL-101(Cr) and 13X zeolite pastes had matured into workable pastes of high plasticity, they were extruded individually on a single screw extruder into monoliths. Then, the extruded MIL-101(Cr) and 13X zeolite monoliths were dried in a cool chamber of controlled temperature (5 °C) and humidity (> 95% relative humidity) for at least a week to achieve uniform drying. When MIL-101(Cr) and 13X zeolite monoliths have dried completely, they were fired in a kiln at 205 °C for 33 hours and 34 minutes for MIL-101(Cr) monoliths and at 400 °C for 41 hours and 27 minutes for 13X zeolite monoliths. The firing step was to sinter adsorbent and clay binder (calcium bentonite) crystals together and to decompose the pore former (licowax C micropowder PM) to form a porous and solidified structure. After the firing process, the fired MIL-101(Cr) monoliths were cooled to room temperature and cut into 10 cm lengths. This was the longest length of MIL-101(Cr) monoliths that were made in this study due to the

amount of MIL-101(Cr) required. For 13X zeolite monoliths, they were cut into 10 cm and 20 cm lengths. Both MIL-101(Cr) and 13X zeolite monoliths prepared in the study (Fig. 2) have square channels with equal wall thickness and channel diameter of 0.90 mm.

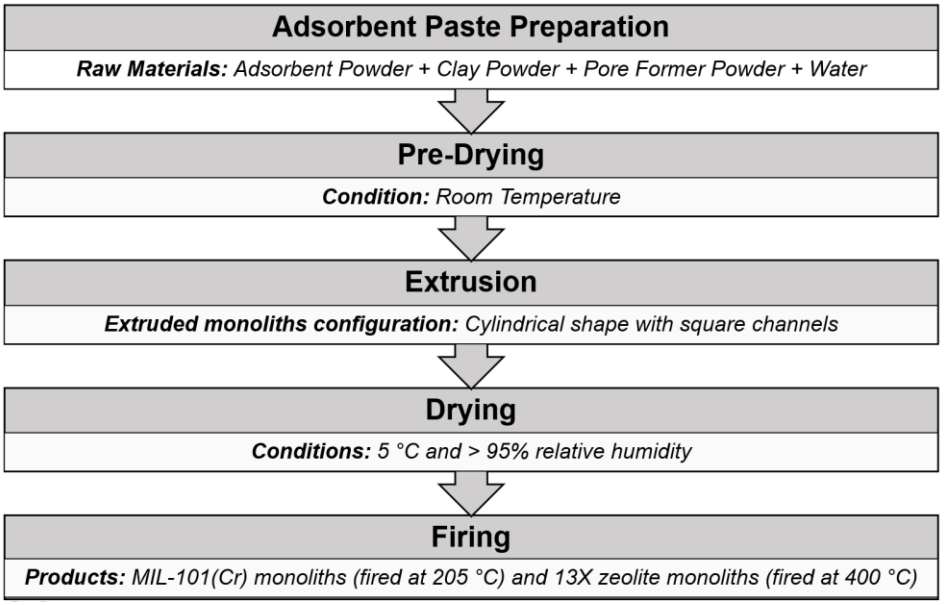


**Fig. 1.** Process scheme of manufacturing MIL-101(Cr) and 13X zeolite monoliths.

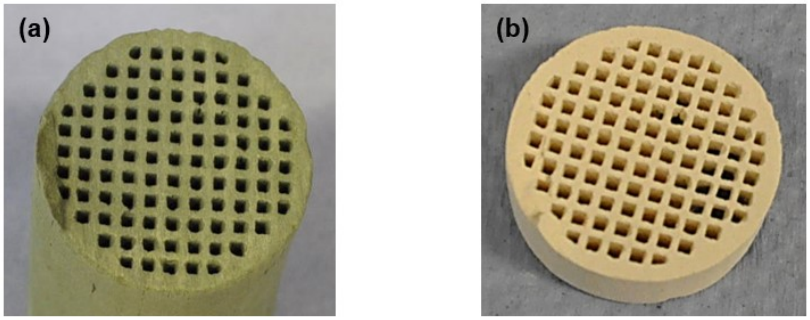


**Fig. 2.** Photographs of (a) MIL-101(Cr) and (b) 13X zeolite monoliths.

## *2.4. Characterization methods*

### *2.4.1. Thermogravimetric and differential scanning calorimetry*

Thermal stabilities of MIL-101(Cr) and 13X zeolite were analysed using a simultaneous thermogravimetric (TG) and differential scanning calorimetric (DSC) analyser (model: Setaram

TGA 92) that was equipped with a microbalance, a furnace and a 100 $mm^3$ alumina crucible. Powder samples of MIL-101(Cr) and 13X zeolite were loaded into a small alumina crucible individually and weighed on a microbalance inside an insulated furnace at room temperature. This analysis was conducted under heated air with temperature between 20 °C to 900 °C at a rate of 10 °C/min. The recorded thermal data of the samples were corrected with the thermal data of an empty alumina crucible and plotted as TG and DSC curves (weight against temperature and heat flow against temperature, respectively).

### *2.4.2. Pore size distribution*

Pore properties of the MIL-101(Cr) and 13X zeolite monoliths were investigated using mercury intrusion porosimetry (MIP). In this study, a mercury penetrometer (model: Micromeritics AutoPore III) with a 3 $cm^3$ bulb glass penetrometer with stem volume of 1.19 $cm^3$ was used. MIL-101(Cr) and 13X zeolite monoliths were crushed into small pieces and loaded separately into a glass penetrometer. The loaded penetrometer was installed onto the low-pressure port of the penetrometer to evacuate gases from the sample. After the low pressure (0 to 3.45 bar) data was collected, it was transferred to the high-pressure port where mercury was forced into the evacuated sample pores at elevated hydraulic pressure up to 4137 bar.

### *2.4.3. Adsorption studies*

Adsorption performance of MIL-101(Cr) and 13X zeolite monoliths for $CO_2$ capture was studied by carrying out dynamic adsorption experiments on an adsorption flow breakthrough apparatus, as shown in Fig. 3. The apparatus consists of a feed gas flow system, an adsorption column and an effluent gas analytical system. Compressed air was used as the purging gas for cleaning the gas streams after each experiment. Considering the difference in thermal stability of MIL-101(Cr) and 13X zeolite crystals, MIL-101 (Cr) and 13X zeolite monoliths were activated in heated air at 150 °C and 250 °C, respectively, for at least 18 hours prior to the

start of each adsorption experiment to remove water and any gas molecules from the pores of the adsorbents.

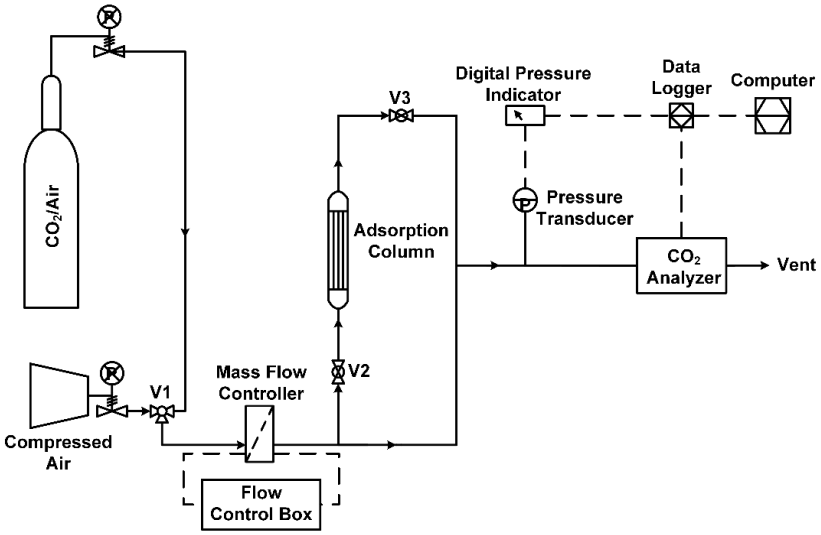


**Fig. 3.** Schematic diagram of an adsorption flow breakthrough apparatus.

The effect of feed gas concentrations was investigated by exposing 10 cm long MIL-101(Cr) monoliths and 20 cm long 13X zeolite monoliths to 0.4% vol., 4% vol. and 40% vol. $CO_2$. Due to the difference in bed length used, the adsorption breakthrough curve was normalised when comparing MIL-101(Cr) and 13X zeolite monoliths. Next, the effect of regeneration temperature on the adsorption properties of sample monoliths (of same bed length of 10 cm) was studied by regenerating them at 150 °C, 180 °C and 200 °C for MIL-101(Cr) monoliths and at 150 °C, 200 °C and 250 °C for 13X zeolite monoliths. These regeneration temperatures were chosen such that they were below their thermal stability temperature, 275 °C for MIL-101(Cr) powder [1] and 800 °C for 13X zeolite powder [18], to ensure there is no phase change of MIL-101(Cr) and 13X zeolite or degradation in their crystal structures. All adsorption experiments were carried out by supplying a constant feed gas flow of 500 mL/min at 2 bar (absolute) at room temperature (~ 20 °C). The change in concentration with time was recorded by a data logger and the experimental adsorption data was plotted as adsorption breakthrough curves.

Important adsorption properties of MIL-101(Cr) and 13X zeolite monoliths such as breakthrough and equilibrium times as well as breakthrough and equilibrium adsorption capacities and effectiveness of the adsorbent bed utilisation can be determined from their $CO_2$ adsorption breakthrough curves. Breakthrough time, $t_b$, is the time at which the effluent gas concentration starts to increase by about 10% of the feed gas concentration (i.e., $C/C_0 \geq 0.1$) and the equilibrium time, $t_e$, is the time at which the effluent gas concentration is the same as the feed gas concentration or when the adsorbent bed is fully saturated with $CO_2$ (i.e., $C/C_0$ = 1.0) [19]. Both breakthrough and equilibrium times were obtained directly from the adsorption breakthrough curve.

Breakthrough and equilibrium adsorption capacities of $CO_2$ are defined as the amount of $CO_2$ gas adsorbed onto the adsorbent bed at breakthrough and equilibrium points, respectively. The breakthrough adsorption capacity, $q_b$, of $CO_2$ was calculated using equation (1) and the equilibrium adsorption capacity, $q_e$, of $CO_2$ was calculated using equation (2). They are normally expressed in terms of millimole of $CO_2$ being adsorbed per gram of adsorbent (mmol/g).

$$q_b = \frac{F}{m_{ad}}\left(t_b - \sum_{t=0}^{t=t_b}\frac{C}{C_0}dt\right) \quad (1)$$

$$q_e = \frac{F}{m_{ad}}\left(t_e - \sum_{t=0}^{t=t_e}\frac{C}{C_0}dt\right) \quad (2)$$

where $F$ is the molar flow rate of the feed $CO_2$ gas (mmol/s), $m_{ad}$ is the mass of adsorbent (g), $C_0$ is the concentration of the feed $CO_2$ gas (g/m$^3$), $C$ is the concentration of the effluent $CO_2$ gas (g/m$^3$) at time $t$ (s) [20] and the term dt is time intervals.

It was assumed that the adsorbent bed of length $L$ consists of equilibrium section and unused bed. The length of equilibrium section of the adsorbent bed, $LES$ (cm), and the length of unused bed, $LUB$ (cm), can be expressed as [19,21]:

$$LES = L - LUB \tag{3}$$

$$LUB = L\left(\frac{t_s - t_b}{t_s}\right) \tag{4}$$

where $t_s$ is the stoichiometric time (s) at which the area under the breakthrough curve after breakthrough at $t_b$ is equal to the area above the breakthrough curve before equilibrium at $t_e$. It is preferable to have short $LUB$ for efficient utilisation of the adsorbent bed [19]. The effectiveness of the adsorbent bed, $\varpi_{bed}$ (%), utilised for $CO_2$ adsorption can then be determined using:

$$\varpi_{bed} = \frac{LES}{L} \times 100\% \tag{5}$$

## 3. Results and discussion

### *3.1. Thermal properties of MIL-101(Cr) and 13X zeolite*

Thermogravimetric (TG) and differential scanning calorimetric (DSC) curves of MIL-101(Cr) and 13X zeolite powders in Fig.s 4(a) and (b), respectively, showed the change in weight and heat flow as they were heated with increasing temperatures. These thermal data of MIL-101(Cr) and 13X zeolite were used to determine their thermal weight loss and stabilities. The TG curve of MIL-101(Cr) in Fig. 4(a) showed that there were two steps in the weight loss when the samples was heated, similar to that reported by Liang et al., 2013 [22]. The first weight loss of about 39.4% was up to 277 °C (due to loss of water molecules) and the second weight loss of about 45.2% was from 280 °C to 480 °C (due to the decomposition of its framework). The endothermic peak between 100 °C and 200 °C on the DSC curve of MIL-101(Cr) powder was due to the loss of water molecules from MIL-101(Cr) whereas the

exothermic peak above 380 °C on the DSC curve of MIL-101(Cr) powder was due to the decomposition of the MOF. This means that MIL-101(Cr) is thermally stable below 380 °C.

For the 13X zeolite powder, its TG curve in Fig. 4(b) indicated that it has a weight loss (or water content) of 21%, similar as that reported by Mishra, 2007 [23], until 500 °C when water molecules were removed from the heated 13X zeolite. The DSC curve of 13X zeolite powder showed an endothermic peak from 100 °C to 400 °C due to dehydration and an exothermic peak from 400 °C to 700 °C due to recrystallisation. The structural collapse of 13X zeolite crystals occur at temperature above 800 °C [18], as indicated by the sharp exothermic peak of the DSC curve above 800 °C. This means that 13X zeolite is thermally stable below 800 °C.

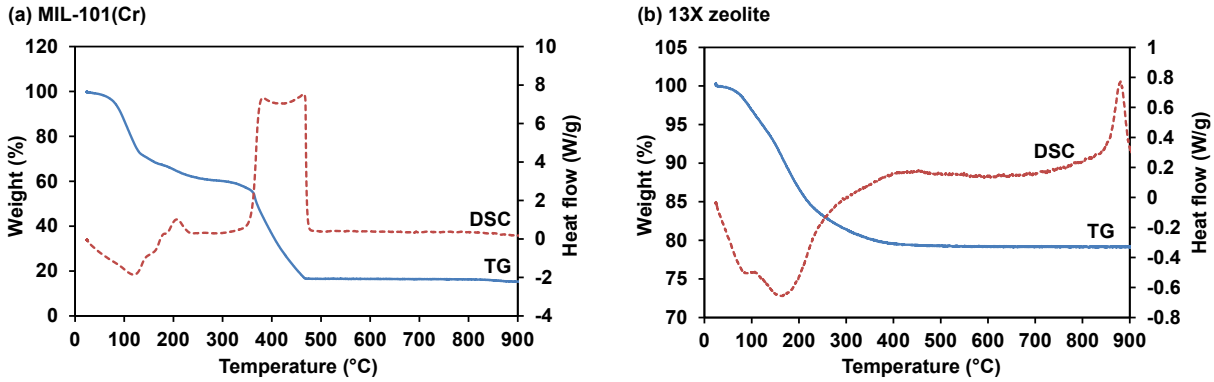


**Fig. 4.** Thermogravimetric (TG) and differential scanning calorimetric (DSC) curves of (a) MIL-101(Cr) and (b) 13X zeolite powders.

### *3.2. Pore structure of MIL-101(Cr) and 13X zeolite monoliths and powders*

The pore properties of MIL-101(Cr) and 13X zeolite monoliths and powders are compared in Table 1. Results indicate that MIL-101(Cr) monoliths have a larger total pore volume (i.e., by about 2.5 times) and total pore surface area (i.e., by about 12.4 times) than 13X zeolite monoliths. The larger total pore volume and total pore surface area of MIL-101(Cr) monoliths means that they have greater storage capacity and greater exposure of adsorption sites for $CO_2$ adsorbate gas compared to 13X zeolite monoliths. However, the study found that

the average pore diameter of MIL-101(Cr) monoliths was about 4.9 times smaller than 13X zeolite monoliths, indicating that some of the cavities of MIL-101(Cr) could be blocked by the calcium bentonite paste. The small average pore diameter of MIL-101(Cr) monoliths means that the penetration of $CO_2$ gas molecules through the pores and the adsorption onto adsorption sites would occur at a slower rate for MIL-101(Cr) monoliths than those for 13X zeolite monoliths.

The total pore volume is generally related to the porosity of the adsorbent structure. Adsorbent monoliths with large total pore volumes tend to have high porosity. Table 1 reveals that the porosity of MIL-101(Cr) monoliths was about 1.3 times higher than 13X zeolite monoliths. The high porosity of MIL-101(Cr) monoliths implies that they have a wider pore network for $CO_2$ adsorbate gas to diffuse into MIL-101(Cr) crystals and adsorb onto adsorption sites located at the surface of the pores as well as those inside the pores than the pore networks in 13X zeolite monoliths. The study also found that MIL-101(Cr) monoliths were less dense than 13X zeolite monoliths. Results in Table 1 show that the bulk density of MIL-101(Cr) monoliths was half of the bulk density of 13X zeolite monoliths.

Reductions in total pore volume (by about 2.5 times), total pore surface area (by about 1.8 times), average pore diameter (by about 1.4 times) and porosity (by about 1.2 times) were indicated in Table 1 when processing MIL-101(Cr) powder into monoliths. These confirmed that access to some MIL-101(Cr) cavities are likely to be blocked by calcium bentonite clay in the monolithic structure. Similarly, due to the same reason, 13X zeolite monoliths have smaller total pore volume (by about half), average pore diameter (by about 0.3 times) and lower porosity (by about 0.8 times) than 13X zeolite powder. Interestingly, the total pore surface area of 13X zeolite monoliths was about 1.7 times larger than that of 13X zeolite powder and this could be due to formation of macropores in the monolithic structure after thermal decomposition of the pore former.

**Table 1**

Pore properties of MIL-101(Cr) and 13X zeolite monoliths and powders.

| Samples | Total pore volume (mL/g) | Total pore surface area ($m^2$/g) | Average pore diameter (nm) | Porosity (%) | Bulk density (g/mL) |
|---|---|---|---|---|---|
| **MIL-101(Cr) monolith** | 1.164 | 195.0 | 23.9 | 65.4 | 0.56 |
| **MIL-101(Cr) powder** | 2.895 | 345.5 | 33.5 | 79.8 | 0.28 |
| **13X zeolite monolith** | 0.464 | 15.7 | 118.0 | 50.8 | 1.10 |
| **13X zeolite powder** | 0.961 | 9.4 | 409.4 | 66.7 | 0.69 |

Pore size distributions of MIL-101(Cr) and 13X zeolite monoliths are shown in Fig. 5. It was seen that both MIL-101(Cr) and 13X zeolite monoliths have larger cumulative pore volume in macropores (pore diameter > 50 nm) than that in mesopores (pore diameter between 2 nm and 50 nm). The cumulative pore volume of MIL-101(Cr) monoliths was found to be larger by about 1.8 times in macropores (likely due to the evaporation of more water molecules in the pre-drying step of the manufacturing of MIL-101(Cr) monoliths) and about the same cumulative pore volume in mesopores when compared to 13X zeolite monoliths. This suggests that the adsorbate $CO_2$ gas molecules are mostly adsorbed in the macropores and less in the mesopores for both MIL-101(Cr) and 13X zeolite monoliths. The variations in their pore volume and distribution of pore sizes were due to the difference in the types of adsorbent materials and thermal treatments used in the manufacturing of MIL-101(Cr) and 13X zeolite monoliths.

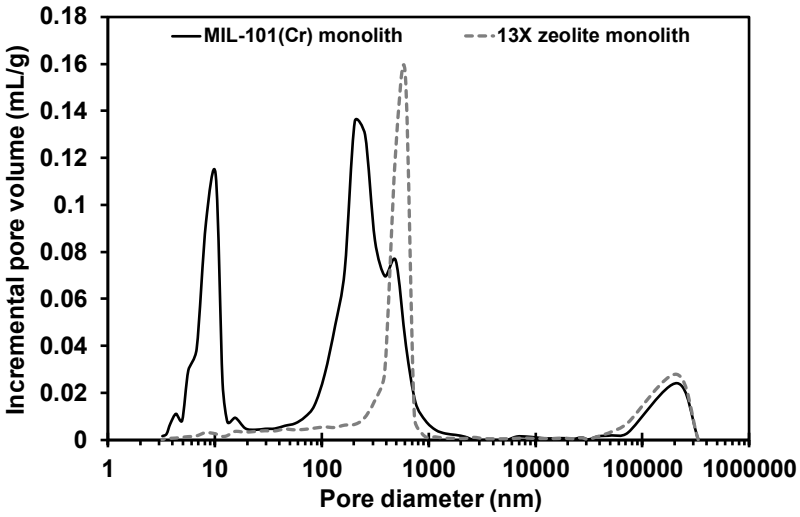


**Fig. 5.** Pore size distributions of MIL-101(Cr) and 13X zeolite monoliths.

### *3.3. $CO_2$ adsorption performances of MIL-101(Cr) and 13X zeolite monoliths*

#### *3.3.1. Effect of varying feed gas concentrations*

Adsorption experiments were carried out with feed $CO_2$ gas concentrations of 0.4%, 4% and 40% vol. at a constant total gas pressure of 2 bar and feed gas flow rate of 500 mL/min. These $CO_2$ gas concentrations correspond to $CO_2$ partial pressure of 0.008 bar, 0.08 bar and 0.8 bar, respectively. The effect of varying feed $CO_2$ gas concentrations are presented in Figs. 6(a) for a MIL-101(Cr) monolith and (b) for a 13X zeolite monolith. It was observed in Figs. 6(a) and (b) that the $CO_2$ adsorption breakthrough curves were steeper at higher feed $CO_2$ gas concentrations. This shows that the mass transfer of $CO_2$ in the adsorbent bed was better at high feed $CO_2$ gas concentration because they have higher $CO_2$ concentration gradient (or $CO_2$ partial pressure) in the adsorbent bed. The mass transfer front reaches the end of the adsorbent bed early and the bed gets saturated with $CO_2$ faster at high $CO_2$ concentration gradient. This was shown by the decrease in breakthrough and equilibrium times when the feed $CO_2$ gas concentration was increased. The study found that the breakthrough time for MIL-101(Cr) monolith was decreased from 2030 s to 641 s and its equilibrium time was decreased from 4053 s to 1834 s when the feed $CO_2$ gas concentration was increased from 0.4% vol. to 4% vol.

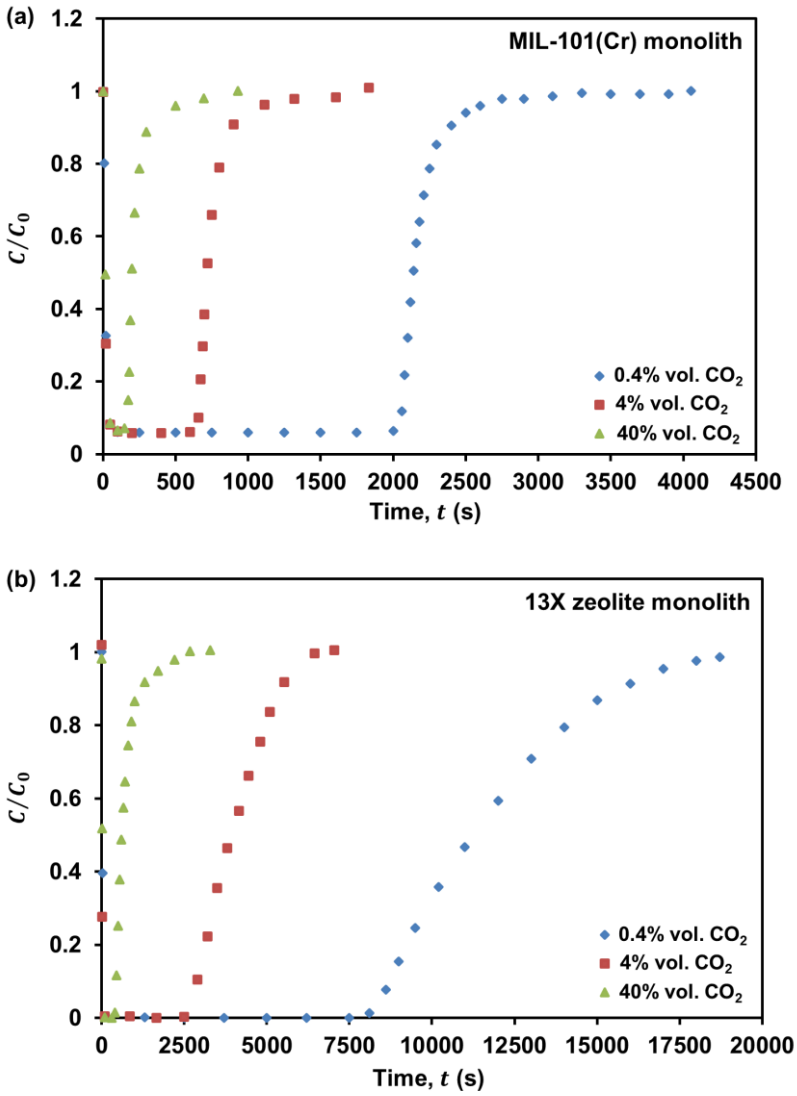


**Fig. 6.** Dynamic adsorption breakthrough curves of 0.4%, 4% and 40% vol. $CO_2$ on (a) MIL-101(Cr) monolith and (b) 13X zeolite monolith at 2 bar and gas flows of 500 mL/min.

Further reduction in breakthrough and equilibrium times was seen when a higher feed $CO_2$ gas concentration (i.e., 40% vol.) was used. For MIL-101(Cr) monoliths, it was found that the breakthrough time was decreased from 641 s to 160 s and the equilibrium time was decreased from 1834 s to 929 s when the feed $CO_2$ gas concentration was increased from 4% vol. to 40% vol. Similar behaviour was observed for 13X zeolite monoliths, in which the breakthrough time was decreased from 8060 s to 396 s and the equilibrium time was decreased from 18720 s to 2675 s when the feed $CO_2$ gas concentration was increased from 0.4% vol. to 40% vol. These results show that the breakthrough and equilibrium times are

affected when there is a change in $CO_2$ concentration gradient (or $CO_2$ partial pressure). A study on $CO_2$ adsorption was conducted by Monazam et al. (2013) [24] using immobilized polyethylenimine (PEI) on mesoporous silica support in a fluid bed and their study showed similar behaviour as that observed here (see Fig. 6). They reported that the breakthrough time was slightly decreased from 570 s to 490 s with steeper breakthrough curves when the feed $CO_2$ concentration was increased from 16.6% vol. to 33.3% vol. Nouh et al. (2010) [25] investigated the effect of varying $CO_2$ concentrations (10% vol., 30% vol. and 70% vol.) on simulated adsorption in a fixed bed adsorption column using an integrated CFD approach and their study showed that the bed was saturated and reached equilibrium faster at a higher feed $CO_2$ concentration.

Table 2 indicates that both breakthrough and equilibrium adsorption capacities of $CO_2$ for MIL-101(Cr) and 13X zeolite monoliths were increased with increasing feed $CO_2$ gas concentration. This was due to the fact that there are more $CO_2$ molecules being adsorbed onto the adsorbent bed at high feed $CO_2$ gas concentration. The study found that the breakthrough adsorption capacity for MIL-101(Cr) monoliths was increased from 0.17 mmol/g to 0.55 mmol/g and its equilibrium adsorption capacity was increased from 0.18 mmol/g to 0.70 mmol/g when the feed $CO_2$ gas concentration was increased from 0.4% vol. to 4% vol. Further increase in the feed $CO_2$ gas concentration from 4% vol. to 40% vol. was found to increase the breakthrough adsorption capacity from 0.55 mmol/g to 1.26 mmol/g and the equilibrium adsorption capacity from 0.70 mmol/g to 1.98 mmol/g for MIL-101(Cr) monoliths. The same trend was seen for 13X zeolite monoliths, in which their breakthrough adsorption capacity was increased from 0.27 mmol/g to 0.98 mmol/g and 1.34 mmol/g and their equilibrium adsorption capacity was increased from 0.40 mmol/g to 1.56 mmol/g and 2.58 mmol/g when the feed $CO_2$ gas concentration was increased from 0.4% vol. to 4% vol. and 40% vol., respectively. This can be explained by the fact that a higher concentration gradient resulted in faster $CO_2$ loading rate on the adsorbent bed due to an increase in the driving force for mass transfer.

**Table 2**

Adsorption properties of MIL-101(Cr) and 13X zeolite monoliths with different $CO_2$ concentrations flowing at a constant pressure of 2 bar and a flow rate of 500 mL/min.

| Samples | $C_0$ (% vol. $CO_2$) | $t_b$ (s) | $t_e$ (s) | $q_b$ (mmol/g) | $q_e$ (mmol/g) | $\varpi_{bed}$ (%) |
|---|---|---|---|---|---|---|
| **MIL-101(Cr) monolith** | 0.4 | 2030 | 4053 | 0.17 | 0.18 | 92.2 |
| | 4 | 641 | 1834 | 0.55 | 0.70 | 80.0 |
| | 40 | 160 | 929 | 1.26 | 1.98 | 67.8 |
| **13X zeolite monolith** | 0.4 | 8060 | 18720 | 0.27 | 0.40 | 68.7 |
| | 4 | 2635 | 7034 | 0.98 | 1.56 | 62.9 |
| | 40 | 396 | 2675 | 1.34 | 2.58 | 53.4 |

The results in Table 2 reveal that the effectiveness of both MIL-101(Cr) and 13X zeolite monolithic adsorbent beds utilised for $CO_2$ adsorption decreases as the feed $CO_2$ gas concentration was increased. The effectiveness of MIL-101(Cr) monolithic adsorbent bed utilised for $CO_2$ adsorption was found to decrease from 92.2% to 80.0% and 67.8% when the feed $CO_2$ gas concentration was increased from 0.4% vol. to 4% vol. and 40% vol., respectively. Similar for 13X zeolite monoliths, the effectiveness of its adsorbent bed utilised for $CO_2$ adsorption (expressed in length percentage) was decreased from 68.7% to 62.9% and 53.4% when the feed $CO_2$ gas concentration was increased from 0.4% vol. to 4% vol. and 40% vol., respectively. The decrease in the utilisation of adsorbent bed for $CO_2$ adsorption are likely to be due to the rapid saturation of the adsorbent bed with $CO_2$ gas molecules at high $CO_2$ concentration gradient due to fast penetration of $CO_2$ gas molecules through the pores and greater adsorption of $CO_2$ in the cavities of MIL-101(Cr) and 13X zeolite.

The $CO_2$ adsorption performances of MIL-101(Cr) and 13X zeolite monoliths are compared and their normalised adsorption breakthrough curves with a feed gas concentration of 40% vol. $CO_2$ are presented in Fig. 7. The total gas pressure and feed gas flow rate were kept constant at 2 bar and 500 mL/min, respectively. It was observed that MIL-101(Cr)

monoliths exhibit a steeper breakthrough curve than 13X zeolite monoliths. This gave an indication that MIL-101(Cr) monoliths have better mass transfer of $CO_2$ in the adsorbent bed than 13X zeolite monoliths due to their highly porous structure, as presented in Section 3.2. As shown in Fig. 7, MIL-101(Cr) monoliths could adsorb up to about 92% vol. of $CO_2$ and 13X zeolite monoliths could adsorb up to about 98% vol. of $CO_2$ from the feed gas stream before they start to breakthrough. This shows that the interactions (van der Waals forces) between $CO_2$ gas molecules and adsorbent surfaces are slightly weaker for MIL-101(Cr) when compared to 13X zeolite, which means $CO_2$ gas molecules can be desorbed from a MIL-101(Cr) monolithic adsorbent bed faster than from a 13X zeolite monolithic adsorbent bed. Tailing of the breakthrough curves was seen as it approaches saturation of adsorbent beds for both MIL-101(Cr) and 13X zeolite monoliths, indicating slow intraparticle diffusion within the pores of the adsorbent particles.

It was also observed that the normalised breakthrough and equilibrium times for MIL-101(Cr) monoliths were shorter than those for 13X zeolite monoliths. This implies that MIL-101(Cr) monoliths get saturated faster and they need more frequent replacement or regeneration than 13X zeolite monoliths. The study found that the normalised breakthrough and equilibrium times for MIL-101(Cr) monoliths were 11.6 s/cm and 119.3 s/cm, respectively. For 13X zeolite monoliths, their normalised breakthrough and equilibrium times were found to be 14.5 s/cm and 182.7 s/cm, respectively. Results in Table 3 reveal that MIL-101(Cr) monoliths have a higher breakthrough adsorption capacity (i.e., by about 37%) but slightly lower equilibrium adsorption capacity (i.e., by about 7%) than 13X zeolite monoliths. This was because most of the adsorption sites in the mesoporous cavities of MIL-101(Cr) monoliths were quickly occupied by $CO_2$ gas molecules at breakthrough and less adsorption sites remained for $CO_2$ adsorption at equilibrium.

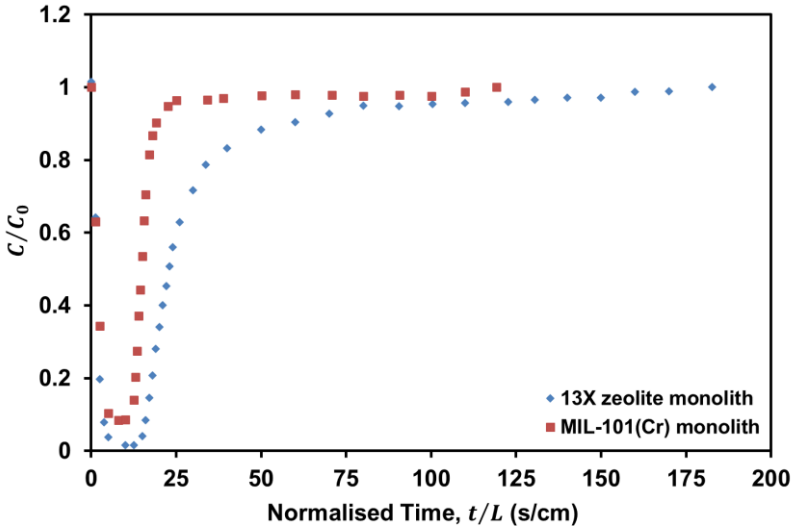


**Fig. 7.** Normalised adsorption breakthrough curves of 40% vol. $CO_2$ on MIL-101(Cr) and 13X zeolite monoliths at 2 bar and gas flows of 500 mL/min.

**Table 3**

Adsorption properties of MIL-101(Cr) and 13X zeolite monoliths with $CO_2$ concentration of 40% vol. at a constant pressure of 2 bar and a feed gas flow rate of 500 mL/min.

| Samples | $t_b$ (s/cm) | $t_e$ (s/cm) | $q_b$ (mmol/g) | $q_e$ (mmol/g) | $\varpi_{bed}$ (%) |
|---|---|---|---|---|---|
| **MIL-101(Cr) monolith** | 11.6 | 119.3 | 1.11 | 1.87 | 65.7 |
| **13X zeolite monolith** | 14.5 | 182.7 | 0.81 | 2.02 | 43.9 |

The presence of calcium bentonite in MIL-101(Cr) and 13X zeolite monoliths prepared in this study was likely to block some of the adsorbent pores and for this reason it was expected that their equilibrium adsorption capacities of $CO_2$ would be lower than those reported in the literature, which is for pure MIL-101(Cr) and 13X zeolite powders. The pure $CO_2$ adsorption isotherm presented by Liang et al (2013) has shown that the equilibrium adsorption capacity of $CO_2$ for their synthesised MIL-101(Cr) powder (of the same chemical formulation as this study) was 2.70 mmol/g at 2 bar and 25 °C [22], which was higher than the value obtained in the present study (i.e., 1.87 mmol/g at the same gas pressure and near to the operating temperature of 21 °C for MIL-101(Cr) monolith) (refer Table 3). Some researchers have reported lower $CO_2$ adsorption capacity than the value obtained in this study. Teo et al. (2017)

performed pure $CO_2$ adsorption on their synthesised MIL-101(Cr) powder (that included concentrated hydrochloric acid in the synthesis) by a volumetric method and showed a $CO_2$ adsorption capacity of 1.60 mmol/g at 2 bar and 25 °C [26]. A similar $CO_2$ adsorption study was conducted by Anbia et al. (2012) and their results showed a much lower $CO_2$ adsorption capacity of 0.20 mmol/g at 2 bar and 25 °C for their synthesised MIL-101(Cr) powder (that has included hydrofluoric acid in the synthesis) [27] when compared to the value obtained in this study (refer Table 3). These results demonstrated that preparative route can affect the $CO_2$ adsorption capacity of MIL-101(Cr).

Furthermore, Garshasbi et al. (2017) has presented a pure $CO_2$ adsorption isotherm for commercial 13X zeolite powder that showed a higher $CO_2$ adsorption capacity of 4.00 mmol/g at 2 bar and 25 °C [28] than the present study, which was 2.02 mmol/g at 2 bar and 25 °C with 40% vol. $CO_2$ for 13X zeolite monolith (Table 3). In terms of adsorbent bed utilisation for $CO_2$ adsorption, the study found that MIL-101(Cr) monoliths were utilised more effectively for $CO_2$ adsorption (i.e., by about 1.5 times) compared to 13X zeolite monoliths. As indicated in Table 3, the effectiveness of the adsorbent bed utilised for $CO_2$ adsorption was found to be 65.7% for MIL-101(Cr) monoliths and 43.9% for 13X zeolite monoliths. This was due to the efficient mass transfer of $CO_2$ in MIL-101(Cr) monoliths, as indicated by the steep breakthrough curve in Fig. 7.

### *3.3.2. Effect of regeneration temperature*

The effect of regeneration temperature on $CO_2$ adsorption performances of MIL-101(Cr) and 13X zeolite monoliths was investigated in this study by carrying out adsorption experiments with feed $CO_2$ gas concentrations of 40% vol. at a constant total gas pressure of 2 bar and feed gas flow rate of 500 mL/min. MIL-101(Cr) monoliths were regenerated at 150 °C, 180 °C and 200 °C and 13X zeolite monoliths were regenerated at 150 °C, 200 °C and 250

°C. The adsorption breakthrough curves for MIL-101 (Cr) and 13X zeolite monoliths are shown in Figs. 8(a) and (b), respectively.

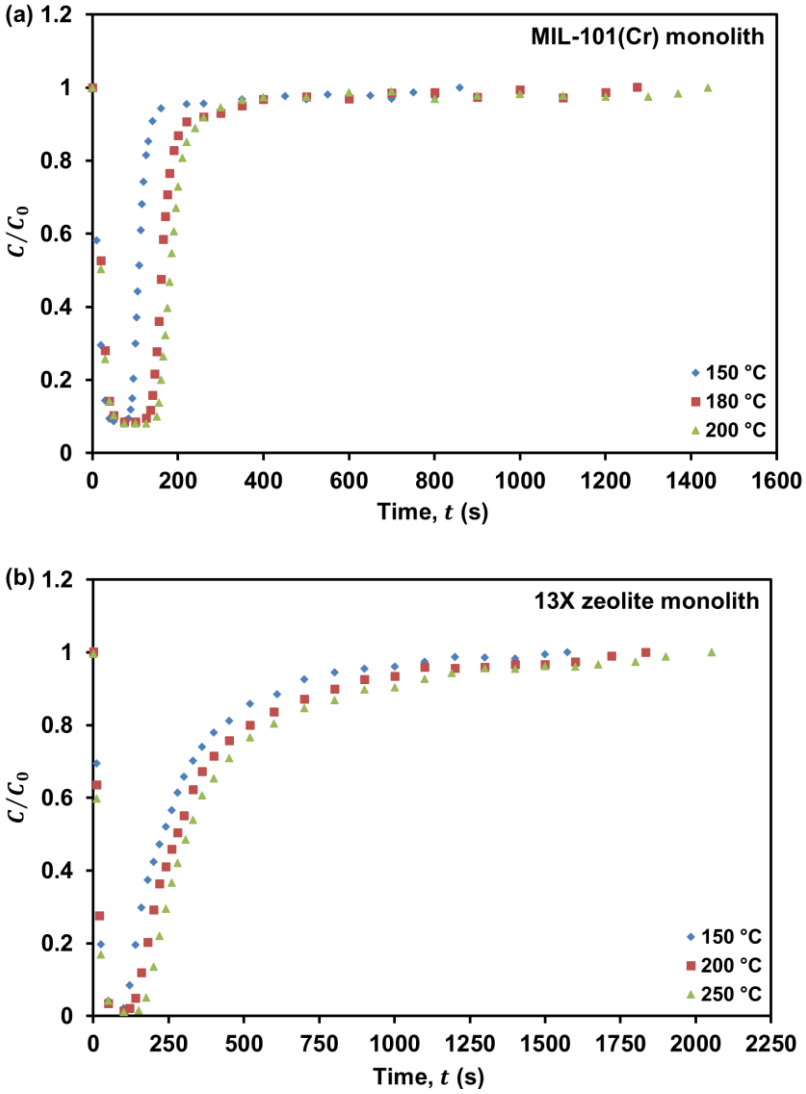


**Fig. 8.** Dynamic adsorption breakthrough curves of 40% vol. $CO_2$ on (a) MIL-101(Cr) monoliths that have been regenerated at 150 °C, 180 °C and 200 °C and (b) 13X zeolite monoliths that have been regenerated at 150 °C, 200 °C and 250 °C at 2 bar and gas flows of 500 mL/min.

As can be seen, the steepness of the breakthrough curves was similar for all regeneration temperatures for both MIL-101(Cr) and 13X zeolite monoliths. This demonstrates that the mass transfer of $CO_2$ in both MIL-101(Cr) and 13X zeolite monoliths was not affected by the regeneration temperature. The breakthrough and equilibrium times for MIL-101(Cr) and 13X zeolite monoliths were found to increase with increasing regeneration temperature, as

shown in Figs. 8(a) and (b) and Table 4. The study found that the breakthrough time for MIL-101(Cr) monoliths was increased from 115 s to 130 s and 149 s and its equilibrium time was increased from 1145 s to 1273 s and 1439 s when the regeneration temperature was elevated from 150 °C to 180 °C and 200 °C, respectively. Similarly for 13X zeolite monoliths, the breakthrough time was found to increase from 105 s to 130 s and 159 s and the equilibrium time was found to increase from 1573 s to 1825 s and 2053 s when the regeneration temperature was elevated from 150 °C to 200 °C and 250 °C, respectively. This implies that MIL-101(Cr) and 13X zeolite monoliths that have been regenerated at high temperature can be used for a longer time for $CO_2$ adsorption before they need to be replaced or regenerated. This was due to the high availability of adsorption sites for $CO_2$ adsorption when the adsorbent bed was subjected to high temperature.

**Table 4**

Adsorption properties of MIL-101(Cr) and 13X zeolite monoliths with different regeneration temperatures for 40% vol. $CO_2$ adsorption at a constant pressure of 2 bar and a feed gas flow rate of 500 mL/min.

| Samples | $T_{regen}$ (°C) | $t_b$ (s) | $t_e$ (s) | $q_b$ (mmol/g) | $q_e$ (mmol/g) | $\varpi_{bed}$ (%) |
|---|---|---|---|---|---|---|
| **MIL-101(Cr) monolith** | 150 | 115 | 1145 | 1.16 | 1.92 | 66.5 |
| | 180 | 130 | 1273 | 1.28 | 2.10 | 67.0 |
| | 200 | 149 | 1439 | 1.52 | 2.38 | 69.1 |
| **13X zeolite monolith** | 150 | 105 | 1573 | 0.58 | 2.01 | 32.9 |
| | 200 | 130 | 1825 | 0.79 | 2.62 | 33.2 |
| | 250 | 159 | 2053 | 1.01 | 3.12 | 35.1 |

Results in Table 4 indicate that the breakthrough and equilibrium adsorption capacities of $CO_2$ for both MIL-101(Cr) and 13X zeolite monoliths increased with increasing regeneration temperature. The study found that the breakthrough adsorption capacity of $CO_2$ for MIL-101(Cr) monoliths was increased from 1.16 mmol/g to 1.28 mmol/g and 1.52 mmol/g and its

equilibrium adsorption capacity of $CO_2$ was increased from 1.92 mmol/g to 2.10 mmol/g and 2.38 mmol/g when the regeneration temperature was elevated from 150 °C to 180 °C and 200 °C, respectively. For 13X zeolite monoliths, their breakthrough adsorption capacity of $CO_2$ was increased from 0.58 mmol/g to 0.79 mmol/g and 1.01 mmol/g and their equilibrium adsorption capacity of $CO_2$ was increased from 2.01 mmol/g to 2.62 mmol/g and 3.12 mmol/g when the regeneration temperature was elevated from 150 °C to 200 °C and 250 °C, respectively. This was because there are more adsorption sites available for $CO_2$ adsorption as a result of efficient desorption of $CO_2$ at higher temperature. Li et al. (2013) [29] and Sayılgan et al. (2016) [30] have also reported the same effect of regeneration temperature on adsorption capacity as the present study.

Since the availability of adsorption sites for $CO_2$ adsorption was increased at higher regeneration temperature, the utilisation of MIL-101(Cr) and 13X zeolite monolithic adsorbent beds for $CO_2$ adsorption was slightly improved when their regeneration temperature was increased, as indicated in Table 4. The study found that the effectiveness of MIL-101(Cr) monolithic adsorbent bed utilised for $CO_2$ adsorption was increased from 66.5% to 67.0% and 69.1% when the regeneration temperature was elevated from 150 °C to 180 °C and 200 °C, respectively. For 13X zeolite monoliths, the effectiveness in utilising the adsorbent bed for $CO_2$ adsorption was found to increase from 32.9% to 33.2% and 35.1% when the regeneration temperature was elevated from 150 °C to 200 °C and 250 °C, respectively.

## 4. Conclusions

MIL-101(Cr) and 13X zeolite monoliths have been successfully manufactured according to novel formulations. The study has validated that MIL-101(Cr) and 13X zeolite powders used in the study were thermally stable up to 380 °C and 800 °C, respectively. MIL-101(Cr) monoliths were found to have larger total pore surface area (by about 12.4 times) and higher porosity (by about 1.3 times) than 13X zeolite monoliths. With these pore characteristics, MIL-

101(Cr) monoliths showed a better $CO_2$ adsorption performance (37% higher in $CO_2$ adsorption capacity at breakthrough with a feed $CO_2$ gas concentration of 40% vol. at 2 bar and feed gas flow of 500 mL/min) than 13X zeolite monoliths. It has been found that $CO_2$ adsorption capacities of MIL-101(Cr) and 13X zeolite monoliths were improved by increasing the feed gas concentration and regenerating them at a higher temperature. The study has demonstrated that MIL-101(Cr) and 13X zeolite monoliths can potentially be used for industrial $CO_2$ capture applications.

## Acknowledgements

This work was financially supported by the Brunei Government. The authors thank Dr Olivier Camus for general laboratory assistance at the Department of Chemical Engineering, University of Bath, United Kingdom.

## References

[1] G. Férey, C. Mellot-Draznieks, C. Serre, F. Millange, J. Dutour, S. Surbie, I. Margiolaki, Science 309 (2005) 2040-2042.

[2] A.R. Millward, O.M. Yaghi, J. Am. Chem. Soc. 127 (2005) 17998-17999.

[3] A. Rehman, S. Farrukh, A. Hussain, E. Pervaiz, Energy Environ. 31 (2019) 367-388.

[4] P. Chowdhury, C. Bikkina, S. Gumma, J. Phys. Chem. C 113 (2009) 6616-6621.

[5] W. Shi, Y. Zhu, C. Shen, J. Shi, G. Xu, X. Xiao, R. Cao, Micropor. Mesopor. Mat. 285 (2019) 129-136.

[6] P. Küsgens, M. Rose, I. Senkovska, H. Fröde, A. Henschel, S. Siegle, S. Kaskel, Micropor. Mesopor. Mat. 120 (2009) 325-330.

[7] Y. Li, R.T. Yang, Langmuir 23 (2007) 12937-12944.

[8] Q. Liu, L. Ning, S. Zheng, M. Tao, Y. Shi, Y. He, Sci. Rep. 3 (2013) 1-6.

[9] S. Ye, X. Jiang, L.W. Ruan, B. Liu, Y.M. Wang, J.F. Zhu, L.G. Qiu, Micropor. Mesopor. Mat. 179 (2013) 191-197.

[10] K. Munusamy, G. Sethia, D.V. Patil, P.B.S. Rallapalli, R.S. Somani, H.C. Bajaj, Chem. Eng. J. 195-196 (2012) 359-368.

[11] R.S. Luciano, Structured Zeolite Adsorbents for $CO_2$ Separation, Luleå University of Technology, 2012. Master Thesis.

[12] F. Rezaei, P. Webley, Chem. Eng. Sci. 64 (2009) 5182-5191.

[13] W.Y. Hong, S.P. Perera, A.D. Burrows, Micropor. Mesopor. Mat. 214 (2015) 149-155.

[14] B.D. Crittenden, W.J. Thomas, Adsorption Technology and Design, Butterworth-Heinemann, Oxford, 1998.

[15] S. Sircar, A.L. Myers, Gas Separation by Zeolites, in: S.M. Auerbach, K.A. Carrado, P.K. Dutta (Eds.), Handbook of Zeolite Science and Technology, Marcel Dekker, New York, 2003, pp. 1063-1104.

[16] H.J. Bart, U.V. Gemmingen, Adsorption, in: Ullmann's Encyclopedia of Industrial Chemistry, Wiley-VCH Verlag GmbH & Co. KGaA, Weinheim, 2012.

[17] S. Cavenati, C.A. Grande, A.E. Rodrigues, J. Chem. Eng. Data 49 (2004) 1095-1101.

[18] C.Y. Li, L.V.C. Rees, Zeolites 6 (1986) 60-65.

[19] J.J. Collins, Chem. Eng. Prog. S. 63 (1967) 31-35.

[20] J.D. Seader, E.J. Henley, Separation Process Principles, John Wiley, New York; Chichester, 1998.

[21] W.L. McCabe, J.C. Smith, P. Harriott, Adsorption and Fixed-Bed Separation, in: Unit Operations of Chemical Engineering, seventh ed. McGraw-Hill, Boston; London, 2005, pp. 836-863.

[22] Z. Liang, M. Marshall, C.H. Ng, A.L. Chaffee, Energy & Fuels 27 (2013) 7612-7618.

[23] D. Mishra, J. Environ. Res. Develop. 1 (2007) 365-368.

[24] E.R. Monazam, J. Spenik, L.J. Shadie, Chem. Eng. J. 223 (2013) 795-805.

[25] S.A. Nouh, K.K. Lau, A.M. Shariff, J. Appl. Sci. 10 (2010) 3229-3235.

[26] H.W.B. Teo, A. Chakraborty, S. Kayal, Appl. Therm. Eng. 110 (2017) 891-900.

[27] M. Anbia, V. Hoseini, J. Nat. Gas Chem. 21 (2012) 339-343.

[28] V. Garshasbi, M. Jahangiri, M. Anbia, Appl. Surf. Sci. 393 (2017) 225-233.

[29] Y. Li, H. Yi, X. Tang, F. Li, Q. Yuan, Chem. Eng. J. 229 (2013) 50-56.

[30] Ş.Ç. Sayılgan, M. Mobehi, S. Ülkü, Micropor. Mesopor. Mat. 224 (2016) 9-16.